J Mater Sci (2007) 42:7757–7761
DOI 10.1007/s10853-007-1628-4

Fabrication and characterization of Ge nanocrystalline growth by ion implantation in SiO_2 matrix

S. N. M. Mestanza · I. Doi · J. W. Swart · N. C. Frateschi

Received: 4 November 2005 / Accepted: 20 February 2007 / Published online: 3 June 2007
© Springer Science+Business Media, LLC 2007

Abstract Ge nanocrystallites (Ge-nc) have been formed by ion implantation of Ge^{+74} into SiO_2 matrix, thermally grown on p-type Si substrates. The Ge-nc are examined by Raman spectroscopy, photoluminescence (PL) and Fourier transform infrared spectroscopy (FTIR). The samples were prepared with various implantation doses [0.5; 0.8; 1; 2; 3; 4] $\times 10^{16}$ cm^{-2} with 250 keV energy. After implantation, the samples were annealed at 1,000 °C in forming gas atmosphere for 1 h. Raman intensity variation with implantation doses is observed, particularly for the peak near 304 cm^{-1}. It was found that the sample implanted with a doses of 2×10^{16} cm^{-2} shows maximum photoluminescence intensity at about 3.2 eV. FTIR analysis shows that the SiO_2 film moved off stoichiometry due to Ge^{+74} ion implantation, and Ge oxides are formed in it. This result is shown as a reduction of GeO_x at exactly the doses corresponding to the maximum blue-violet PL emission and the largest Raman emission at 304 cm^{-1}. This intensity reduction can be attributed to a larger portion of broken Ge–O bonds enabling a greater number of Ge atoms to participate in the cluster formation and at the same time increasing the oxygen vacancies. This idea would explain why the FTIR peak decreases at the same implantation doses where the PL intensity increases.

S. N. M. Mestanza (✉) · I. Doi · J. W. Swart · N. C. Frateschi
Center for Semiconductor Components,
State University of Campinas,
P. O. Box 6061, 13083-870 Campinas, SP, Brazil
e-mail: nilo@ccs.unicamp.br

N. C. Frateschi
Department of Applied Physic,
Institute of Physic Gleb-Wataghing,
State University of Campinas,
P. O. Box 6165, CEP 13084-970 Campinas, SP, Brazil

Introduction

In recent years, semiconductors nanocrystals have attracted great interest for potential applications in electronic and optoelectronic devices [1, 2]. The main reason for this interest is that such structures show efficient charge storage capacity in discrete memory devices (transistor floating gate) [3] and visible photoluminescence at room temperature (RT) [4], besides its compatibility with silicon-based integrated circuit technology. Specifically Ge-nc embedded in SiO_2 matrix, shows advantages with respect to Si: strong quantum confinement [5] resulting in a direct gap semiconductor nature, high dielectric constant, and smaller band-gap [2].

Ge-nc embedded in SiO_2 can be obtained by preparation techniques such as laser ablation [6], LPCVD [7], ion implantation [8], and rf co-sputtering [9]. We have chosen the technique of ion implantation due to its simplicity and compatibility with integrated circuit technology, and because of the simplicity of controlling particle size and density. In the ion implantation technique Ge-nc can be produced by implanting Ge ions at high doses into SiO_2 matrix, following by high temperature annealing to induce precipitation and the formation of the Ge-nc. In this paper we study the effects of the implantation doses on the crystalline ordering of the Ge-nc formed in SiO_2 matrix. Samples were investigated using Raman spectroscopy, PL and FTIR.

Experiment

SiO_2 films with a thickness of 300 nm were grown on (100) p-Si substrates, with a resistivity of 4 Ω cm, using thermal oxidation at 1,000 °C, for 90 min. Monte Carlo simulation

code (TRIM) was used to calculate the adequate energy in order to place the maximum Ge concentration at the middle of the SiO_2 film. SiO_2 matrices were implanted with Ge^{74+} ions at RT, with 250 keV energy, using implantation doses of [0.5, 0.8, 1, 2, 3 and 4] × 10^{16} cm^{-2}. After ion implantation, the samples were annealed at 1,000 °C for 1 h in a forming gas atmosphere to precipitate Ge and to form the nanocrystallites.

Raman spectra were obtained using a triple grating T-64000 Jobin-Yvon spectrometer, with 1 cm^{-1} spectral resolution. The 514 nm line of the argon laser was used to excite the samples. All samples were measured at RT; the laser power on the sample was 9 mW. The diameter of the laser spot was 50 μm and the integration time was 30 min. The resonant Raman spectra were obtained in the back-scattering configuration. The orientation of the Si substrate is fundamental to polarize the laser light, allowing the second-order Raman Si peak, at about 300 cm^{-1}, to be suppressed not masking the Raman peaks corresponding to Ge-nc.

PL spectra were measured at RT with a 240 nm excitation source, using a Spex Fluoromax spectrometer with a R298 Hamamatsu photomultiplier.

Compositional analysis of the SiO_2 matrix was carried out using a DIGILAB infra-red Fourier transform spectrometer. The system was purged with dry N_2 to reduce the infrared (IR) absorption from H_2O and CO_2. Transmittance measurements were carried out within the 400–4,000 cm^{-1} range at 300 K. The beam spot size was about 5 mm diameter and the resolution was 4 cm^{-1}. In all cases a non-processed Si substrate sample was used as a reference.

Results and discussions

Figure 1 presents the Raman spectra of the films implanted with various doses [0.5; 0.8; 1; 2; 3; 4] × 10^{16} cm^{-2}, followed by annealing forming-gas, (92% N_2 + 8% H_2) at 1,000 °C, for 1 h. The position of the peak for bulk Ge was determined at 302.4 cm^{-1} and this value is used to compare with Ge-nc peaks. The Raman spectra of the implanted samples clearly show three bands: 210–280, 304 and 430 cm^{-1}. The first one, 210–280 cm^{-1}, is associated with amorphous Ge compounds. Such band was expected as the samples have been annealed at 1,000 °C, therefore above the Ge melting temperature (938.3 °C) [10]. At this temperature, Ge precipitates as liquid droplets inside a viscous oxide matrix. The second band was near 304 cm^{-1}, and can be associated with Ge-nc. This band is in good agreement with the work reported by Wu et al. [11]. Finally, the third band at 430 cm^{-1} is related to local Si–Si vibrations [12].

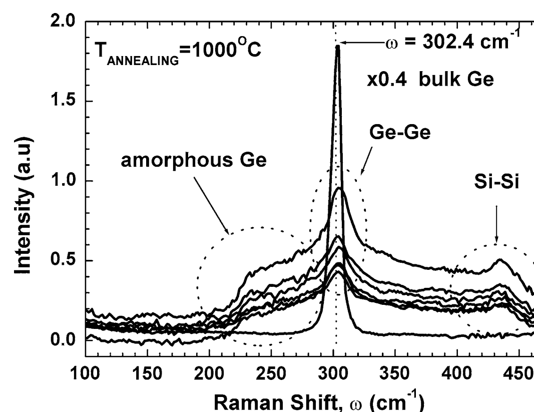

Fig. 1 Raman spectra at room temperature for Ge-nc embedded in SiO_2 matrix as a function of implantation doses. The Raman spectra in these samples show clearly three bands: 210–280, 304 and 430 cm^{-1} associated with Ge amorphous, Ge-nc and Si–Ge localized, respectively

Figure 2 shows in detail the second band at about 304 cm^{-1} for all samples. In this figure we can observe the followings: (a) all spectra present a well-defined peak and their shapes are essentially the same as observed for bulk Ge crystal (c-Ge). The presence of this band in our spectra confirms the existence of Ge-nc in the SiO_2 matrix. (b) All Raman spectra not only show wider, but also slightly antisymmetrical and blue shifts bands, when comparing to bulk c-Ge. The displacement in the position of the Raman peak for Ge-nc, according to Wellner et al. [13], can be attributed to isotopic effects, phonon confinement and stress effects of the oxide matrix on the Ge-nc. (c) All Raman spectra show a variation of the position of the maximum intensity peak near w~304 cm^{-1} with

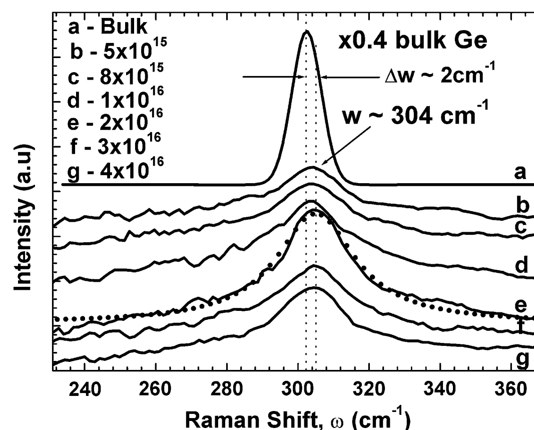

Fig. 2 Room temperature Raman spectra of Ge^+-implanted in SiO_2 matrix with doses of (b) 5 × 10^{15}, (c) 8 × 10^{15}, (d) 1 × 10^{16}, (e) 2 × 10^{16}, (f) 3 × 10^{16}, and (g) 4 × 10^{16} ions/cm^2. For comparison the spectrum of the Ge-bulk was included in (a). The bulk spectrum has been multiplied by 0.4 for clarity

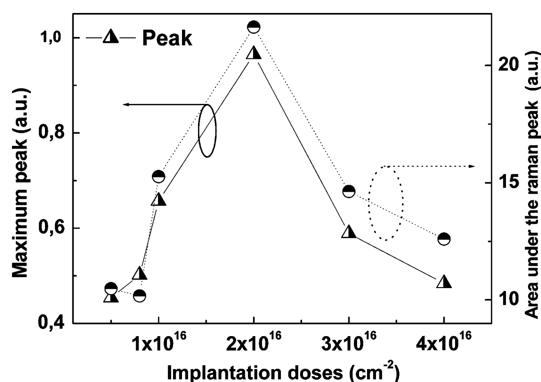

Fig. 3 Maximum intensity peak and area under the Raman curve as a function of Ge^{+} implantation doses

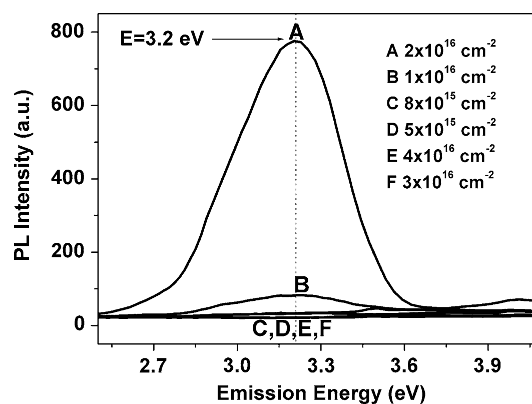

Fig. 4 PL spectra obtained for samples annealed at 1,000 °C for 1 h after RT-implantation at an energy of 250 keV with doses of 5×10^{15}, 8×10^{15}, 1×10^{16}, 2×10^{16}, 3×10^{16}, 4×10^{16} cm^{-2}

implantation doses, see Fig. 3. This effect leads us to believe that the implantation doses can exerts influence in the level of crystallinity of the nanostructures and damages produced inside the oxide matrix and not hilled by the annealing could be affecting the Raman intensity. (d) Finally the maximum Raman intensity occurs for doses of 2×10^{16} cm^{-2}.

Figure 3 shows the maximum peak and area under the Raman peak as a function of Ge^{+} implantation doses. Comparing these results, it is observed that both the area and the Raman intensity exhibit a maximum at implantation doses of 2×10^{16} cm^{-2}. Simple Lorentzian fitting have been made on the Raman spectra in order to obtain the peak position, full width at half maximum (FWHM), and the area under the Raman peak, see Table 1. The FWHM of the Raman spectra has an average value of 17 nm. The FWHM values indicate reasonable crystallinity when compared with previous reports [11]. Using the results of the FWHM dependence with average particle size from Fujii et al. [14], we can estimate the average nanostructure sizes to be between 4 and 5 nm. A possible explanation for the large FWHM value in the present case can be attributed to the polycrystalline effect in the silicon oxide matrix

Table 1 Measured Raman peak position ω, FWHM $\Delta\omega$ and area under the Raman peak

Doses (cm^{-2})	ω (cm^{-1}) Lorentzian	FWHM $\Delta\omega$ (cm^{-1})	Area (a.u.)
5×10^{15}	305.1	14.3	10.48
8×10^{15}	304.5	15.8	10.17
1×10^{16}	304.3	20.2	15.26
2×10^{16}	304.5	17.2	21.64
3×10^{16}	304.7	19.1	14.63
4×10^{16}	304.1	16.6	12.6
Bulk Ge	302.4	8.3	–

caused by the high annealing temperature. Another explanation might be related to implantation-induced lattice disorder.

Figure 4 shows the room temperature PL spectra for Ge-implanted at different implantation doses and annealing at 1,000 °C for 1 h. The spectra exhibit a broad blue-violet PL band at around 3.2 eV (400 nm) and a weak peak at about 4.0 eV. In our experiment, maximum PL intensity was achieved with implantation doses of 2×10^{16} cm^{-2}. The weak emission was only observed for the doses of 1×10^{16} and 2×10^{16} cm^{-2}. Maximum PL intensity peak was reached at implantation doses of 2×10^{16} cm^{-2}, approximately 10 times higher than that at the 1×10^{16} cm^{-2} doses. Similar behavior has been reported by Lee et al. [15]. However, the origin of this PL band and the relationship to Ge-nc is not clear. It has been observed in the literature that the PL band at about 3.2 eV is due to germanium–oxygen-deficient-centers (GODC) [16, 17]. In our opinion, we believe that the PL emission is more related to these defects and the annealing temperature than to the emission from Ge-nc excitonic transitions.

Figure 5 shows a typical change of FTIR absorption spectral of Ge-nc embedded in a SiO_2 matrix. All spectra show three well defined sharp peaks around ~460, ~840 and ~1,080 cm^{-1}, associated with rocking, bending and stretching vibration modes of the Si–O bonding, respectively [18]. Studies reported in the literature have shown that Ge implanted SiO_2 matrix followed by high annealing temperatures leads to a process of germanium oxide formation [19]. From this set of FTIR spectra, we observe clearly the presence of GeO_x peak by the presence of vibration modes at around 600 cm^{-1}. This peak is associated with the Ge–O–Ge bending mode and is present in all the implanted and annealed samples. The peak position is shifted by 20 cm^{-1} when compared to previous reports [18, 20]. Lucovsky et al. [21] has shown detailed studies of

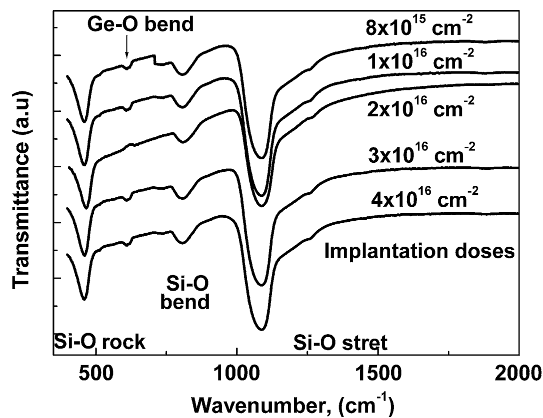

Fig. 5 FTIR transmission spectra for samples annealed at 1,000 °C for 1 h after RT-implantation at an energy of 250 keV with doses of 5×10^{15}, 8×10^{15}, 1×10^{16}, 2×10^{16}, 3×10^{16}, 4×10^{16} cm^{-2}. In the stoichiometric SiO_2 film, tree vibrational bands exist at 460, 840 and 1,080 cm^{-1} (TO_3 mode), corresponding to rocking, bending and asymmetric stretching vibrations of Si–O–Si bond, respectively

the influence of several SiO_x film deposition parameters in the vibrational frequencies. Zacharias et al. [22] has also pointed out the existence of a high concentration of oxygen in the sample as being the reason for a 60 cm^{-1} displacement observed in the Ge–O–Ge stretching mode.

In our opinion, the discrepancy observed in the position of the Ge–O FTIR peak is more likely associated with differences in fabrication technique and parameters used to produce the GeO_x. In SiO_2, for instance, it is well known that depending on the fabrication technique, the film thickness, and pressure in the deposition chamber, the Si–O stretching can shift up to 100 cm^{-1} [23].

A detailed examination of the Ge–O–Ge bending mode shows a slight reduction exactly at the same implantation doses for which we have obtained the maximum PL and Raman emission. A possible explanation for the reduction in intensity for these doses is that a larger portion of the Ge atoms is participating in cluster formation. At the same time, PL spectra indicate that a larger number of oxygen vacancies might occur for these same doses. Thus, we believe this may be an indication that GeO_x formation is probably inhibiting both the cluster and the vacancy defect development. This study is ongoing and is still not clear the mechanism by which this process can occur.

Conclusion

We have studied the optical and structural characteristics of Ge nanocrystallites obtained by ion implantation and annealing at high temperatures. In these results it was observed that Ge nanocrystallites coexist with amorphous Ge at annealing temperatures of 1,000 °C. A photoluminescence peak at 3.2 eV and Raman spectrum at 304 cm^{-1} are observed for the sample implanted at room temperature with doses of 2×10^{16} cm^{-2}. The origin of the PL emission is most probably due to GODC defects produced both during the implantation and annealing processes. Analysis of the Infrared spectroscopy indicates a slight intensity reduction in GeO_x at exactly the doses 2×10^{16} cm^{-2}. A possible explanation for this reduction at this particular implantation doses is that a higher portion of the Ge–O bonds are being broken enabling a greater number of Ge atoms to participate in the cluster formation. We believe that the shift in the Ge–O peaks in the FTIR is more associated with differences in the technique and parameters used to produce the GeO_x.

Acknowledgment The authors would like to acknowledge Dr M. Behar of IF/UFRGS for his help with ion implantation, Dr J. M. J. Lopez for his help with the PL measurements and Dr E. Granado and A. Garcia, IFGW/UNICAMP, for the Raman spectroscopy measurements. This work was supported by the Conselho Nacional de Desenvolvimento Científico e Tecnológico (CNPQ).

References

1. Giri PK, Kesavamoorthy R, Panigrahi BK, Nair KGM (2005) Solid State Commun 133:229
2. Rebohle L, Von Borany J, Yankov RA, Skorupa W, Tyschenko IE, Frob H, Leo K (1997) Appl Phys Lett 71:2809
3. Choi WK, China WK, Heng CL, Teo LW, Ho V, Ng V, Antoniadis DA, Fitzgerald EA (2002) Appl Phys Lett 80:2014
4. Pavesi L, Dal Negro L, Mazzoleni C, Franzo G, Priolo F (2000) Nature 408:440
5. Bostedt C, Van Burren T, Willey TM, Franco N, Terminello LJ, Heske C, Moller T (2004) Appl Phys Lett 84:4056
6. Yoshida T, Takeyama S, Yamada Y, Mutoh K (1996) Appl Phys Part 1 35:94
7. Marins ES, Mestanza SNM, Doi I (2006) Mater Sci Semiconduct Process 9:828
8. Giri PK, Kesavamoorthy R, Panigrahi BK, Nair KGM (2006) Nucl Instr Meth Phys Res B 244:56
9. Hayashi S, Fujii M, Yamamoto K (1989) Jpn J Appl Phys 28 part I:1464
10. Zhu JG, White CW, Budai JD, Withrow SP, Chen Y (1995) J Appl Phys 78:4386
11. Wu XL, Gao T, Yan F, Jiang SS, Feng D (1997) J Appl Phys 82:2704
12. Kolobov AV (2000) J Appl Phys 87:2926
13. Wellner A, Paillard V, Bonafos C, Coffin H, Claverie A, Schmidt B, Heining KH (2003) J Appl Phys 94:5639
14. Fujii M, Hayashi S, Yamamoto K (1990) Appl Phys Lett 57:2692
15. Lee WS, Jeong JY, Kim HB, Chae KH, Whang CN, Im S, Song JH (2000) Mater Sci Eng B 69–70:474
16. Gallagher M, Österberg U (1993) Appl Phys Lett 63:2987

17. Zhang JY, Wu XL, Bao XM (1997) Appl Phys Lett 71:2505
18. Wu XL, Gao T, Siu GG, Tong S, Bao XM (1999) Appl Phys Lett 74:2420
19. Skorupa W, Rebolhe L, Gebel T (2003) Appl Phys A 76:1049
20. Zhang JY, Bao XM, Ye YH (1998) Thin Solid Films 323:68
21. Pai PG, Chao SS, Takagi Y, Lucovsky G (1986) J Vac Sci Technol A 4:689
22. Zacharias M, Blasing J (1995) Phys Rev B 52:14018
23. Alayo MI, Pereyra I, Scopel WL, Fantini MCA (2002) Thin Solid Films 402:154